Life Sciences in Space Research 26 (2020) 69–76

Contents lists available at ScienceDirect

Life Sciences in Space Research

journal homepage: www.elsevier.com/locate/lssr

Investigation of shielding material properties for effective space radiation protection

Masayuki Naito[a], Satoshi Kodaira[a,*], Ryo Ogawara[a,1], Kenji Tobita[a,2], Yoji Someya[a], Tamon Kusumoto[a], Hiroki Kusano[a], Hisashi Kitamura[a], Masamune Koike[a], Yukio Uchihori[a], Masahiro Yamanaka[b], Ryo Mikoshiba[b], Toshiaki Endo[b], Naoki Kiyono[b], Yusuke Hagiwara[b], Hiroaki Kodama[b], Shinobu Matsuo[b], Yasuhiro Takami[b], Toyoto Sato[c], Shin-ichi Orimo[c,d]

[a] Space Quantum Research Group, QST Advanced Study Laboratory, National Institutes for Quantum and Radiological Science and Technology, Chiba 263-8555, Japan
[b] Space Systems Division, Integrated Defense & Space Systems, Mitsubishi Heavy Industries, Ltd., Aichi 455-8515, Japan
[c] Institute for Materials Research, Tohoku University, Sendai 980-8577, Japan
[d] WPI-Advanced Institute for Material Research (AIMR), Tohoku University, Sendai 980-8577, Japan

ARTICLE INFO

Keywords:
Radiation dose
Radiation protection
Shielding material

ABSTRACT

Geant4 Monte Carlo simulations were carried out to investigate the possible shielding materials of aluminum, polyethylene, hydrides, complex hydrides and composite materials for radiation protection in spacecraft by considering two physical parameters, stopping power and fragmentation cross section. The dose reduction with shielding materials was investigated for Fe ions with energies of 500 MeV/n, 1 GeV/n and 2 GeV/n which are around the peak of the GCR energy spectrum. Fe ions easily stop in materials such as polyethylene and hydrides as opposed to materials such as aluminum and complex hydrides including high *Z* metals with contain little or no hydrogen. Attenuation of the primary particles in the shielding and fragmentation into more lightly charged and therefore more penetrating secondary particles are competing factors: attenuation acts to reduce the dose behind shielding while fragmentation increases it. Among hydrogenous materials, $^{6}Li^{10}BH_4$ was one of the more effective shielding materials as a function of mass providing a 20% greater dose reduction compared to polyethylene. Composite materials such as carbon fiber reinforced plastic and SiC composite plastic offer 1.9 times the dose reduction compared to aluminum as well as high mechanical strength. Composite materials have been found to be promising for spacecraft shielding, where both mass and volume are constrained.

1. INTRODUCTION

Manned space explorations are currently being carried out in the International Space Station (ISS) and will soon extend to the Moon and beyond. Space crew members are exposed to space radiation consisting of energetic charged particles, which can cause harmful radiation effects. ISS operates in in low-Earth orbit (LEO) and so crews are partially shielded from galactic cosmic rays (GCRs) and solar energetic particles (SEPs) by the geomagnetic field. Beyond LEO the radiation environment is hostile because magnetic shielding as provided in LEO is practically absent. On the planned Lunar Orbital Platform Gateway (Crusan et al., 2018) and on future missions to Mars and deep space, space crews will be exposed to much higher space radiation levels due to the long flight durations. The accumulated dose equivalent in free space for round-trip travel to Mars is expected to be ~660 mSv from GCRs based on the assumption of a 180 day one way duration and similar flight conditions and similar shielding as for the Mars Science Lab (MSL) cruise with additional highly variable contributions from SEP events (Zeitlin et al., 2013). Radiation shielding is one of the radiation countermeasures under consideration as human operations are extended, into deep space.

The US National Aeronautics and Space Administration (NASA) has described health hazards to humans during space activities (Cucinotta, 2015). Exposure to protons and high atomic number and high energy (HZE) particles from He to Fe nuclei in GCRs increases radiation risks. The HZE particles contribute substantially to the radiation dose due to high linear energy transfer (LET), resulting in significant biological effects even if contributions of HZE particles to the

* Corresponding author: Satoshi Kodaira, Ph.D., National Institutes for Quantum and Radiological Science and Technology, Chiba 263-8555, Japan
E-mail address: kodaira.satoshi@qst.go.jp (S. Kodaira).
[1] Current address: Advanced Research Center for Beam Science, Institute for Chemical Research, Kyoto University, Kyoto 611-0011, Japan
[2] Current address: School of Engineering, Tohoku University, Sendai 980-8579, Japan

https://doi.org/10.1016/j.lssr.2020.05.001
Received 16 March 2020; Received in revised form 7 May 2020; Accepted 8 May 2020

GCR composition are small (e.g. Cucinotta, 2014). Dosimetry in the space environment has been carried out in manned missions in the Apollo era (English et al., 1973), the space shuttle (e.g. Badhwar *et al.*, 1996; Doke *et al.*, 2001), the Mir station (e.g. Beaujean *et al.*, 2002) and the ISS (e.g. Ambrozova *et al.*, 2011; Kodaira *et al.*, 2013; Berger *et al.*, 2016). Crews on the Lunar Orbital Platform Gateway will encounter much higher radiation dose rates compared with the crews in missions in LEO.

Dose reduction strategies in space including passive shielding, active shielding and reducing mission durations have been investigated in several studies (e.g. Durante, 2014). One of the practical solutions to reduce space radiation dose is the use of shielding materials attenuating HZE particles, i.e. passive shielding. HZE particles lose their energies via electromagnetic interactions or breakup into lighter nuclei and neutrons through nuclear fragmentation in the shielding materials. While it is not feasible to completely stop all high energy particles in the shielding materials because of their extremely long ranges. A passive shield can reduce radiation dose. The shielding effects of various materials such as aluminum (Al) and polyethylene (PE, $(C_2H_4)_n$) have been verified by accelerator beam experiments on the ground (e.g. Miller et al., 2003; La Tessa et al., 2005; Guetersloh et al., 2006; Zeitlin et al., 2006; DeWitt et al., 2009). Hydrogen is the most effective element for obtaining large shielding efficiency per mass density (e.g. Wilson *et al.*, 1997; Zeitlin *et al.*, 2005), but it is not easy to handle and not stable. On the ISS dose reductions by PE blocks and packages made of water soaked sanitary towels have been investigated (Shavers et al., 2004; Kodaira et al., 2014).

In this paper, we investigated the space radiation properties of several materials as a function of two parameters, stopping power and nuclear fragmentation cross section using a Monte Carlo simulation in the Geant4 toolkit (Agostinelli et al., 2003; Allison et al., 2006; Allison et al., 2016).

2. MATERIALS AND PARAMETERS

2.1. Shielding parameters: stopping power and fragmentation cross section

Here, the two physical parameters for radiation protection are described. The first parameter is S, the stopping power of a material, which is defined by the Bethe-Bloch equation,

$$S = \frac{dE}{dx} \propto NZ_T, \tag{1}$$

where E and x are, respectively, the particle energy and depth in the medium, N is the number of molecules per unit volume and Z_T is the atomic number of the target material. The S contributes to moderation of charged particles in the target material. The stopping power per unit density is obtained by dividing S by the material density ρ,

$$\frac{S}{\rho} \propto \frac{Z_T}{A_T}, \tag{2}$$

Here, A_T is the atomic mass of the target material. S is ~1/2 for many elements, but it is 1 for hydrogen. In the case of a chemical compound, the stopping power is described as

$$\frac{S}{\rho} \propto \frac{\sum N_i Z_{Ti}}{\rho} \propto \frac{Z_{Ttotal}}{A_T}, \tag{3}$$

where subscript i represents each element in the compound and Z_{Ttotal} is the sum of the atomic numbers of all elements in a molecule of the compound.

The second parameter is the total nuclear fragmentation cross section. Fragmentation of the primary beam produces more lightly charged and therefore less ionizing secondary particles. However, the total effect on dose due to fragmentation of the primary HZE particles will decrease since the LET of ions with a given energy per nucleon is roughly dependent on its electric charge squared. The cross section of a nuclide $\sigma_{nuclide}$ follows the Bradt-Peters semi-empirical formula. It is roughly described by using A_T and the atomic mass of the primary particle A_p as

$$\sigma_{nuclide} \propto (A_p^{1/3} + A_T^{1/3})^2 \text{increases with } A_T^{2/3}. \tag{4}$$

Note that $\sigma_{nuclide}$ describes only the inclusive fragmentation cross section, which does not take into account the number of secondary particles yielded by the interaction. In considering the total fragmentation cross section of a molecule σ_{mole}, the average atomic mass of the molecule should be used. In other words, A_T has to be replaced by the average atomic mass A_{Tave} with the total number of atoms in the molecule n; i.e. $\sigma_{mole} \propto nA_{Tave}^{2/3}$. For example, σ_{mole} of PE σ_{PE} is obtained by

$$\sigma_{PE} \propto 6 \times \left(\frac{12.01 \times 2 + 1.01 \times 4}{6}\right)^{2/3}. \tag{5}$$

The number of molecules N is required to obtain the material cross section σ_{mat}, and the material cross section per unit density is obtained by dividing σ_{mat} by ρ as well as the stopping power per unit density (Eq. 2) (Durante, 2014),

$$\sigma_{mat} \propto N\sigma_{mole} \propto \frac{\rho n A_{Tave}^{2/3}}{A_T} \propto \frac{\rho A_{Tave}^{2/3}}{A_{Tave}} \propto \frac{\rho}{A_{Tave}^{1/3}}. \tag{6}$$

$$\frac{\sigma_{mat}}{\rho} \propto A_{Tave}^{-1/3}. \tag{7}$$

The idea that hydrogen is the most effective shielding material is based on the relations in (Eq. 3) and (Eq. 7). The shielding efficiency denotes the dose reduction rate for per unit density which follows from Z_{Ttotal}/A_T (Eq. 3) and $A_{Tave}^{-1/3}$ (Eq. 7). Materials with large values of both shielding parameters are favored for space radiation shielding.

2.2. Materials

The target materials as listed in Table 1 were chosen for the purpose of verifying Eqs. 3 and 7 across a range of material compositions. They include Al and materials containing hydrogen, such as PE, hydrides, complex hydrides and composite materials. Current spacecraft are constructed largely of aluminum, and some ISS modules incorporated PE shielding (e.g. Shavers et al., 2004). Hydrides and complex hydrides have been developed as possible solid state hydrogen storage materials for future "hydrogen economy" (e.g. Orimo et al., 2007). These materials release and absorb hydrogen via a reversible reaction depending on the temperature. Some complex hydrides have larger hydrogen concentrations than polyethylene. Other complex hydrides have a large

Table. 1
The density, hydrogen mass fraction, stopping power parameters, and cross section parameters of materials.

Meterial	Group	Density (g/cm^2)	H fraction (wt%)	S	σ_{mat}	Z_{Ttotal}/A_T	$A_{Tave}^{-1/3}$
Al	(iv)	2.7	0.00	1.30	0.90	0.48	0.33
PE	(ii)	0.94	14.40	0.54	0.56	0.57	0.60
LiH	(i)	0.78	12.70	0.39	0.49	0.50	0.63
^{6}LiH	(i)	0.78	14.38	0.44	0.51	0.57	0.66
$LiBH_4$	(i)	0.67	18.51	0.37	0.44	0.55	0.65
$^6Li^{10}BH_4$	(i)	0.67	20.13	0.40	0.45	0.60	0.67
$Li_2B_{12}H_{12}$	(i)	1.18	7.77	0.59	0.65	0.50	0.55
$Li_4BH_4(NH_2)_3$	(i)	0.99	11.14	0.52	0.58	0.53	0.58
NH_3BH_3	(ii)	0.78	19.63	0.45	0.50	0.58	0.64
NH_3	(ii)	0.70	17.19	0.41	0.43	0.59	0.62
$Mg(BH_4)_2$	(ii)	0.78	14.96	0.43	0.46	0.56	0.59
AlH_3	(iii)	1.49	10.10	0.79	0.76	0.53	0.51
MgH_2	(iii)	1.45	7.67	0.77	0.70	0.53	0.48
Mg_2FeH_6	(iv)	2.76	5.47	1.40	1.20	0.51	0.43
Mg_2NiH_4	(iv)	2.71	3.62	1.36	1.08	0.50	0.40
CFRP	(iii)	1.17	8.87	0.63	0.64	0.54	0.55
SCP	(iii)	1.36	7.63	0.73	0.70	0.54	0.52

density with moderate hydrogen concentration. These characteristic features of complex hydrides have the potential for use as radiation shielding. Here, possible hydrides and complex hydrides with various hydrogen concentrations (3.62-20.13 wt%) and densities (0.70-2.76 g/cm^3) were investigated. We also investigated two composite materials, carbon fiber reinforced plastic (CFRP) and SiC composite plastic (SCP). Composite materials are composed of resin and reinforced to enhance mechanical strength. By selecting appropriate resins and reinforcement, the composite material becomes more resistant to shock and heat than the resins and reinforcement separately. They are being used in automobiles, aircraft and spacecraft because of their low density and high mechanical strength (e.g., Chen, 1997). In order to optimize mass in spacecraft, composite materials ideally should be multi-functional, serving as radiation shielding and as strong, light weight spacecraft structures and components. In this work, CFRP and SCP made of C/SiC reinforcements and polypropylene resin ($(C_3H_6)_n$) in a volume ratio of 2:8 were investigated.

2.3. Numerical simulation

Using a monte carlo simulation we investigated the dose reduction for various materials as a function of the two parameters: stopping power and nuclear fragmentation cross section. The production and transport of radiation were calculated using the Geant4 code v10.05.p02 (Agostinelli et al., 2003; Allison et al., 2006; Allison et al., 2016) with the Geant4 reference physics model “Shielding”. This model employs intra-nuclear cascade models of QMD (Koi, 2010), Bertini (Bertini, 1969) and Fritiof (Andersson et al., 1993) for hadronic interactions. Electromagnetic interaction was included by Geant4 standard physics (Agostinelli et al., 2003; Allison et al., 2006; Allison et al., 2016). ENDF/B-VIII.0 (Brown et al., 2018) was chosen as a data library for neutron cross sections.

First, we calculated the GCR elemental contribution to effective dose equivalent in free space in order to find the element contributing to dose. The GCR energy spectra at the 2010 solar minimum were taken from Matthiä et al., 2013. The energy spectra were converted to the effective dose equivalent by fluence-to-dose conversion coefficients for isotropic exposure (ICRP, 2013). The GCR elemental contribution to effective dose equivalent is shown in Fig. 1. The hydrogen and helium contributions are 33.2% and 9.8% of the total, respectively, and the HZE particles contribute the remainder despite their small abundances in the GCR. These contribution ratios are consistent with previous studies of the differences in GCR models, solar modulation and methods used to obtain the effective dose equivalent (e.g. Ballarini et al., 2006; Dobynde and Shprits, 2020). Hydrogen and helium are difficult to shield against due to their low stopping power. Moreover, their contributions increase behind shielding materials due to secondary particles produced by target fragmentation in the shielding material. The reduction of effective dose equivalent due to the HZE particles is important because HZE particles occupy about 50% of the total. Iron nuclei (Z = 26) are the heaviest significant contributors and therefore are milestone commonly used benchmark for shielding effectiveness against GCRs. In this work, we investigated the dose reduction by shielding materials against Fe nuclei with energies of 500 MeV/n, 1 GeV/n and 2 GeV/n spanning the peak of the GCR energy spectrum.

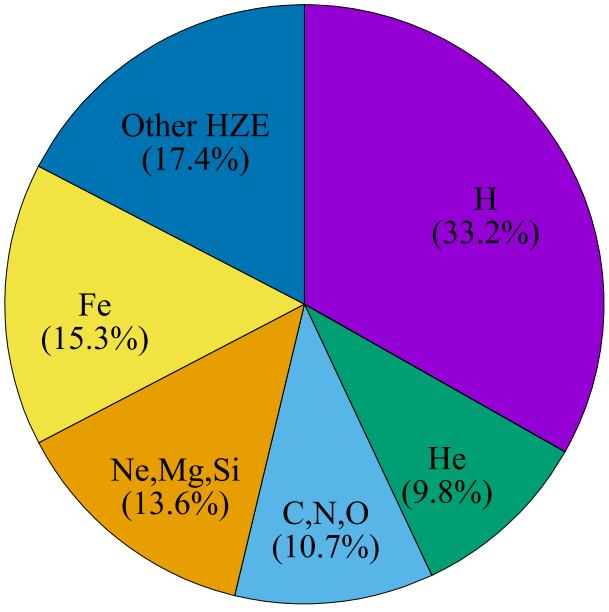

Figure 1. GCR elemental contribution to effective dose equivalent in free space during solar minimum.

The materials were exposed to a mono-energetic iron pencil beam (Fig. 2). Fluence vs. energy spectra of the primary (i.e. Fe ions) and secondary particles (neutrons, electrons, positrons, photons, pions, muons and charged particles) behind the target material (thickness: 0-40 g/cm^2) were calculated. The effective dose equivalent was obtained by using the ICRP conversion coefficient (ICRP, 2013) as well as the GCR elemental contribution.

2.4. Benchmark experiment

To verify the numerical simulations we made measurements at HIMAC (Heavy Ion Medical Accelerator in Chiba) of QST, Japan. Target materials of Al, PE and composite materials (CFRP and SCP) slabs were stacked with CR-39 nuclear track detectors (TechnoTrak, Chiyoda Technol Corp., Japan) for measuring LET distribution (Kodaira et al., 2016). The thickness of the Al slab was 10 mm and the thickness of other materials was 20 mm. The total thickness by stacking target materials ranged from 20 to 60 mm. Each stack was exposed to 500 MeV/n Fe ions with a fluence of 2×10^3 cm^{-2}. (The hydrides and complex hydrides were not available for these measurements.) The procedure for analyzing the CR-39 is described in Kodaira et al., 2016.

LET spectra behind targets of several thicknesses are shown in Fig. 3. The peak around 200 keV/μm (showing as Fe_1) is due to the primary Fe ions registered in CR-39 in front of target materials. The peak LET increases with increasing thickness of target materials due to the ionization energy loss, while the number of counts decreases due to the nuclear fragmentation. Each distribution was fitted with a gaussian function for analyzing the mean LET and number of counts for comparison with the numerical simulation. Figure 4 summarizes the variations of LET and number of Fe counts as a function of target material thickness as obtained by the experiment and simulation. The numerical results are in good agreement with the experimental results within ± 10% except around Bragg-peak, where small trivial differences between the ideal set-up in the simulation and the actual experimental set-up can lead to large differences between simulation and measurement. The results confirm that the numerical simulation generally reproduces the fragmentation and transport of Fe.

3. RESULTS AND DISCUSSION

3.1. Parameters of shielding materials

The shielding parameters of the target materials are summarized in Table 1 and Fig. 5. The shielding efficiency depends on the hydrogen mass fraction in the material as expressed by Eqs. 3 and 7. Shielding efficiency (due to stopping power and fragmentation) and material density is trade-off, in the sense that materials with high shielding efficiency are typically low density. We classified the materials into four groups (i-iv) based on the shielding efficiency and the density. Colors in Fig. 5 represent the four groups.

Group (i) materials (blue) are low density hydrides (0.67-1.18 g/

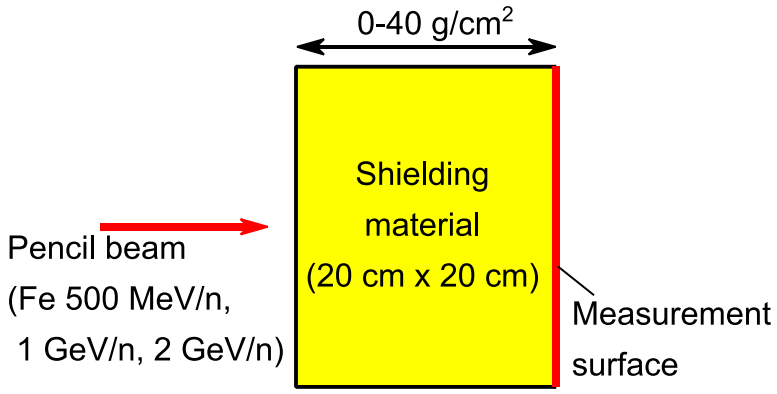

Figure 2. Schematic drawing of the numerical simulation.

cm^3). The shielding efficiency is low in the stopping power parameter (Z_{Ttotal}/A_T) and relatively high in the fragmentation cross section parameter ($A_{Tave}^{-1/3}$). The neutron rich nuclides of ^{7}Li and ^{11}B contained naturally low Z_{Ttotal}/A_T. If these hydrides consist of ^{6}Li and ^{10}B as shown in the open symbol (^{6}LiH and ^{6}Li^{10}BH$_4$), the Z_{Ttotal}/A_T value is to be high. Note that this effect is not related to the neutron capture. ^{6}Li^{10}BH$_4$ has the highest shielding efficiency in this group.

Group (ii) materials (magenta) are low density hydrides (0.70-0.78

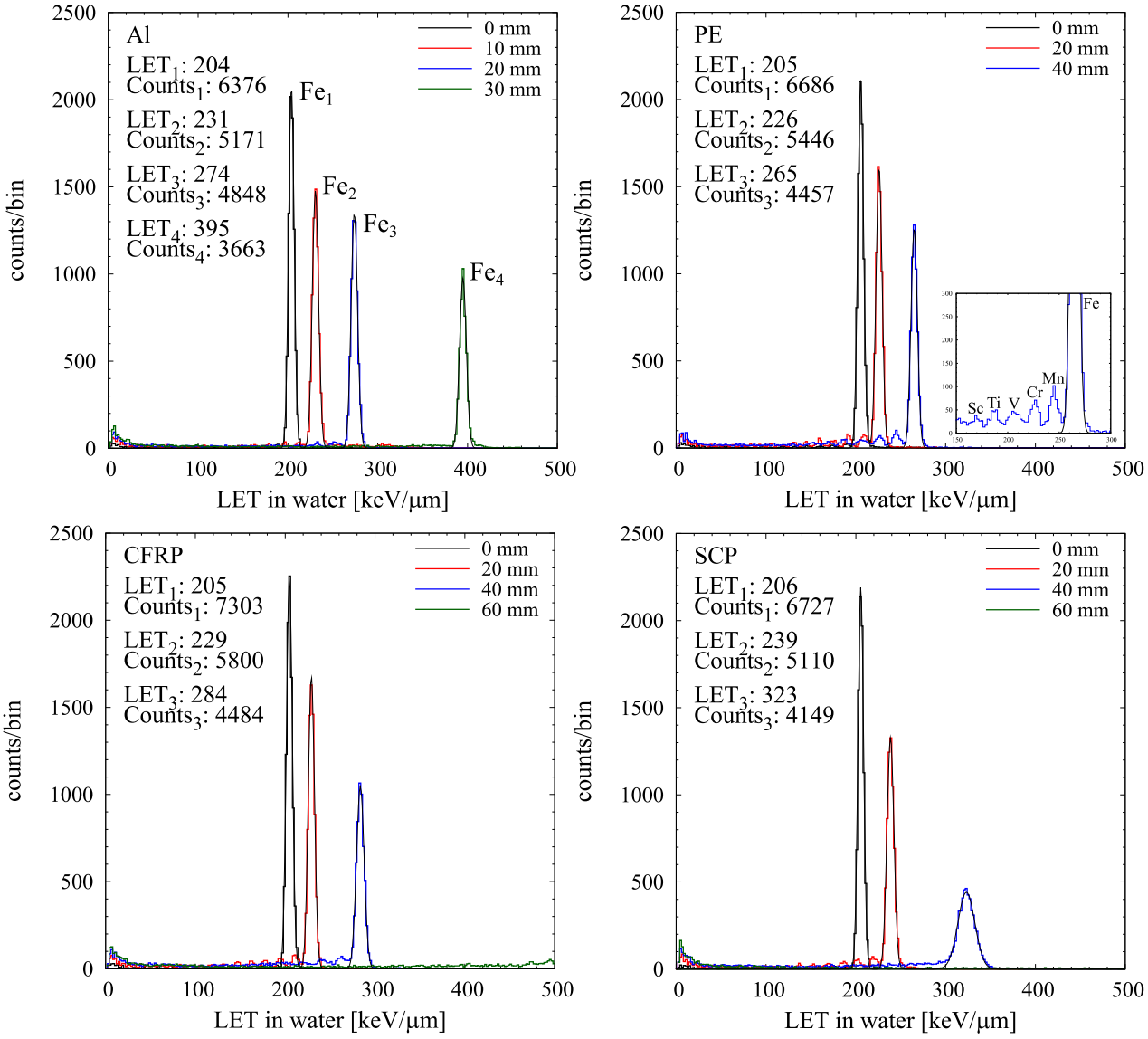

Figure 3. LET spectra behind the targets (Al, PE, CFRP and SCP) of several thicknesses (0 – 60 mm). 0 mm denotes in front of target. Fragments are clearly observed in the enlarged view of PE data for the LET range 150-300 keV/μm.

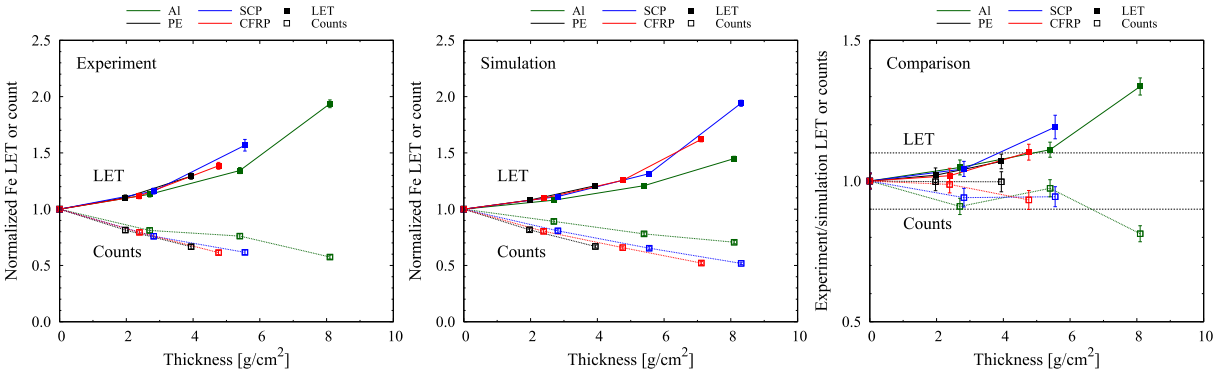

Figure 4. Variations of LET and number of counts of Fe ions as a function of material thickness obtained by experiment (left) and numerical simulation (center). The rightmost panel shows the ratios of experiment to simulation for LET and number of counts. The dotted lines denote ± 10%.

g/cm^3) showing high shielding effectiveness due to the large hydrogen concentration. PE (black), which is conventionally used as a shielding material, is in this group. NH_3 gives better shielding efficiency in this group. However, NH_3 (ammonia) is a hazardous chemical and the liquid ammonia requires careful handling, similar to hydrogen. The use of ammonia in combination with some absorbing materials (Klerke et al., 2008) may provide stability and eliminate the hazardous features so as to make practical and effective materials with high shielding efficiency. NH_3BH_3 is also one of better materials. NH_3 and NH_3BH_3 have a high composition ratio of H:B and/or N of 3:1 an improvement over PE (H:C = 2:1).

Groups (i) and (ii) are low density materials, so a thick material and therefore large total volume is required to obtain significant shielding effect, which may be an issue given the size limitations of spacecraft. (It may however be practical for future lunar and planetary habitats.)

Group (iii) materials (red) are intermediate density (1.17-1.49 g/cm^3) materials, which show intermediate shielding efficiency. The balance between shielding efficiency and material density requires trade studies, given the severe restriction in both mass and volume in spacecraft. The composite materials (CFRP and SCP) are better materials for practical use due to the strong mechanical properties. Spacecraft structures and components made of composite materials will be better for shielding compared with conventional Al. Note that the CFRP and SCP evaluated here are representative examples. Customized composites with different resin, reinforcement and fractions can be evaluated for optimal balancing of shielding and mechanical properties.

Group (iv) materials (cyan) are high density materials (~2.7 g/cm^3), which exhibit low shielding efficiency. The high density offers the favorable property of low volume. Al (green), which is conventionally used in spacecraft, is in this group. Mg_2FeH_6 and Mg_2NiH_4 offer better shielding than Al due to their relatively high hydrogen fraction.

3.2. The effective dose reduction with shielding materials

The variations of effective dose equivalent of total (primary + secondary), primary particles (i.e. Fe ions) and secondary radiations (neutrons, electrons, positrons, photons, pions, muons, and charged ions) as a function of material thickness for 2 GeV/n, 1 GeV/n and 500 MeV/n Fe beams are shown in Fig. 6. The values within each group of materials are very close, so representative materials from each group are shown. The data points are normalized with the data of total effective dose equivalent in front of the target materials (i.e. 0 g/cm^2). The dose reductions generally follow the two shielding parameters. The ranges of Fe ions in the target materials are seen in the data of primary particles (Figs. 6(b), (e) and (h)) depending on the primary particle energies. The difference of range depends on the stopping power

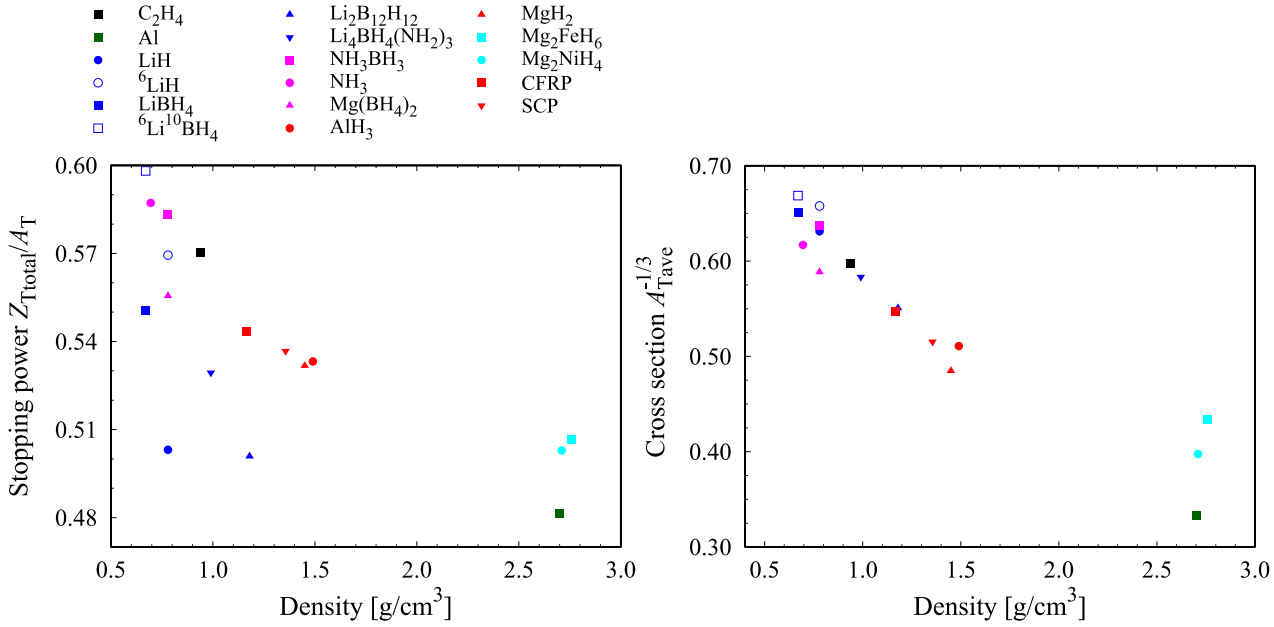

Figure 5. Relationship between material density and shielding parameters of stopping power (left) and fragmentation cross section (right). Hydrides, complex hydrides and composite materials are classified by colors (group (i): blue, (ii): magenta, (iii): red, (iv): cyan, Al: green and PE: black).

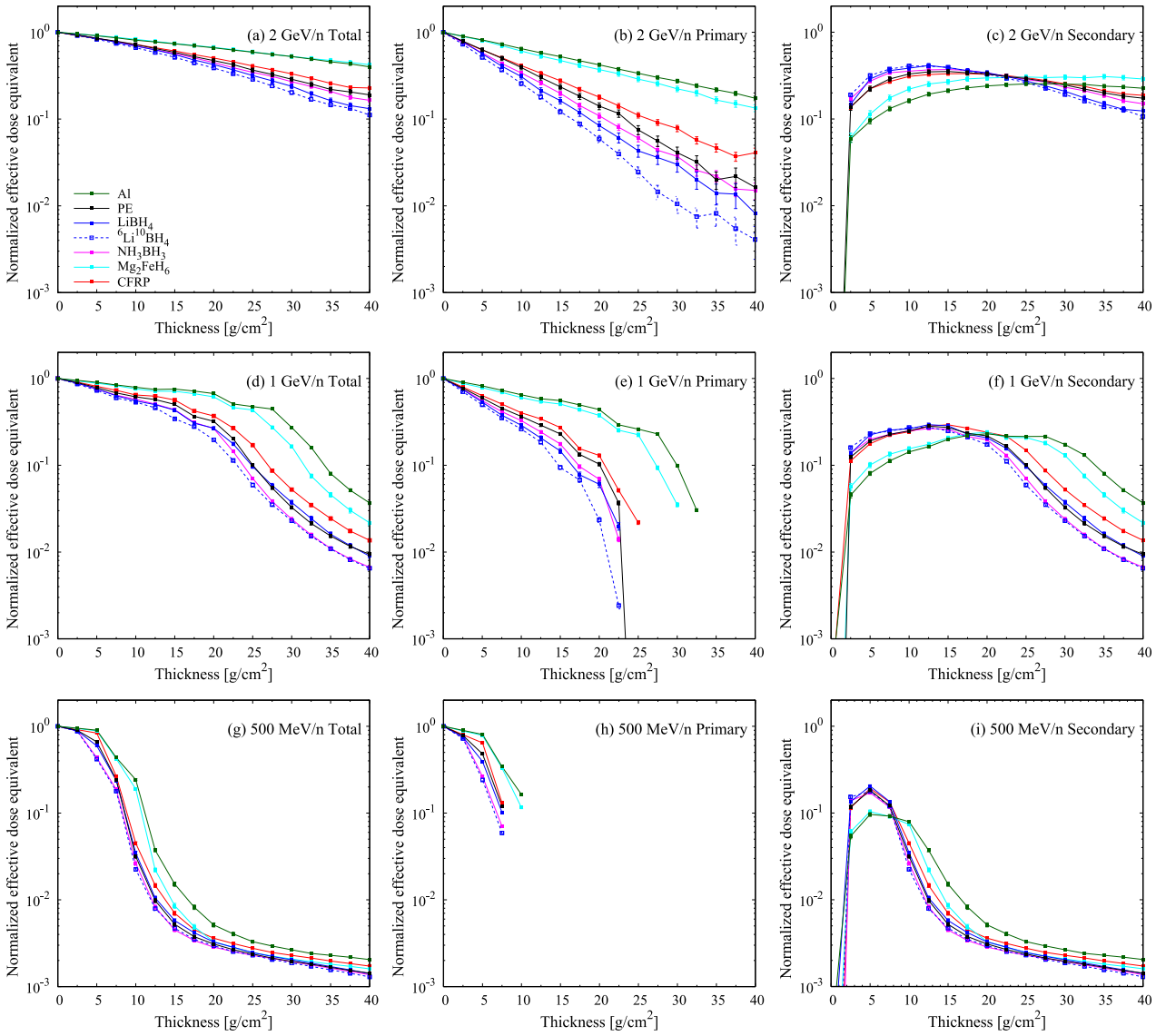

Figure 6. Variations of effective dose equivalent as a function of each material thickness for 2GeV/n (a-c), 1GeV/n (d-f) and 500 MeV/n (g-i) Fe beam simulation. The values within each group of materials are very close, so representative materials from each group are shown. Data points are normalized with the data of total effective dose equivalent at 0 g/cm^2. (a, d and g): Total effective dose equivalent (primary + secondary). (b, e, and h): Primary particles (i.e. Fe). (c, f and i): Secondary radiations such as neutrons, photons, electrons, positrons, pions, muons and charged ions.

parameter of target material as clearly shown in 1 GeV/n data (Fig. 6(e)). Fe ions easily stop in the high hydrogen fraction materials (group (i) and (ii)) as opposed to the materials containing little or no hydrogen (group (iv)). The dose due to secondary radiation increases due to fragmentation and then decreases following the survived number of primary particles (Fig. 6(c), (f) and (i)). The peak of the secondary dose shifts to greater thickness depending on the material density. This is because of the decrease in the fragmentation coefficient (survived number of primary particles for a given depth in the target material) in high density and heavy metal materials (group (iv)). As clearly shown in 2 GeV/n data (Fig. 6(b)), the fragmentation coefficient strongly depends on the cross section in the target material. The dose reduction at 2 GeV/n is dominated by fragmentation, while that of 500 MeV/n Fe ions is dominated by the ionization energy loss. 1 GeV/n data reveal an intermediate situation for both energy loss and fragmentation. The natural-group (i) materials represent high dose reduction rates compared to PE for 2 GeV/n Fe, while the 1 GeV/n data are similar to PE data. This is explained by their high cross section and low stopping power. Although the fragmentation of primary particles decreases the primary dose effectively, the dose from secondary particles is not reduced by energy loss. In accordance with Giraudo *et al.*, 2018, LiH is better than PE for dose reduction as indicated by both calculation and experiment using < 6.1 g/cm^2 LiH target. The results indicate that the thick LiH is not as effective as PE. The idea of multilayered shielding suggested in Giraudo *et al.*, 2018 may be more efficient by combining group (i) and group (ii) materials. We found that the dose reduction rate of ^{6}Li and ^{10}B enriched group (i) materials having high hydrogen fraction are better than natural-group (i) materials and PE due to higher nuclear fragmentation cross section and greater hydrogen fraction.

Figure 7 summarizes and compares the calculation results for 1 GeV/n Fe ions. Figures 7(a) and (b) show the scatter plots of each parameter (stopping power and cross section) and the normalized effective dose equivalent behind the target materials of 20 g/cm^2. Figure 7(c) compares the normalized effective dose equivalent for each material. Figure 7(d) shows a three dimensional view based on Figs. 7 (a) and (b). The higher dose reduction rates of 77.2% and 80.3% were obtained in ^{6}LiH and ^{6}Li^{10}BH$_4$ in the group (i) materials, respectively. ^{6}Li^{10}BH$_4$ is 1.2 times better than PE (67.9%). NH$_3$BH$_3$ in the group (ii)

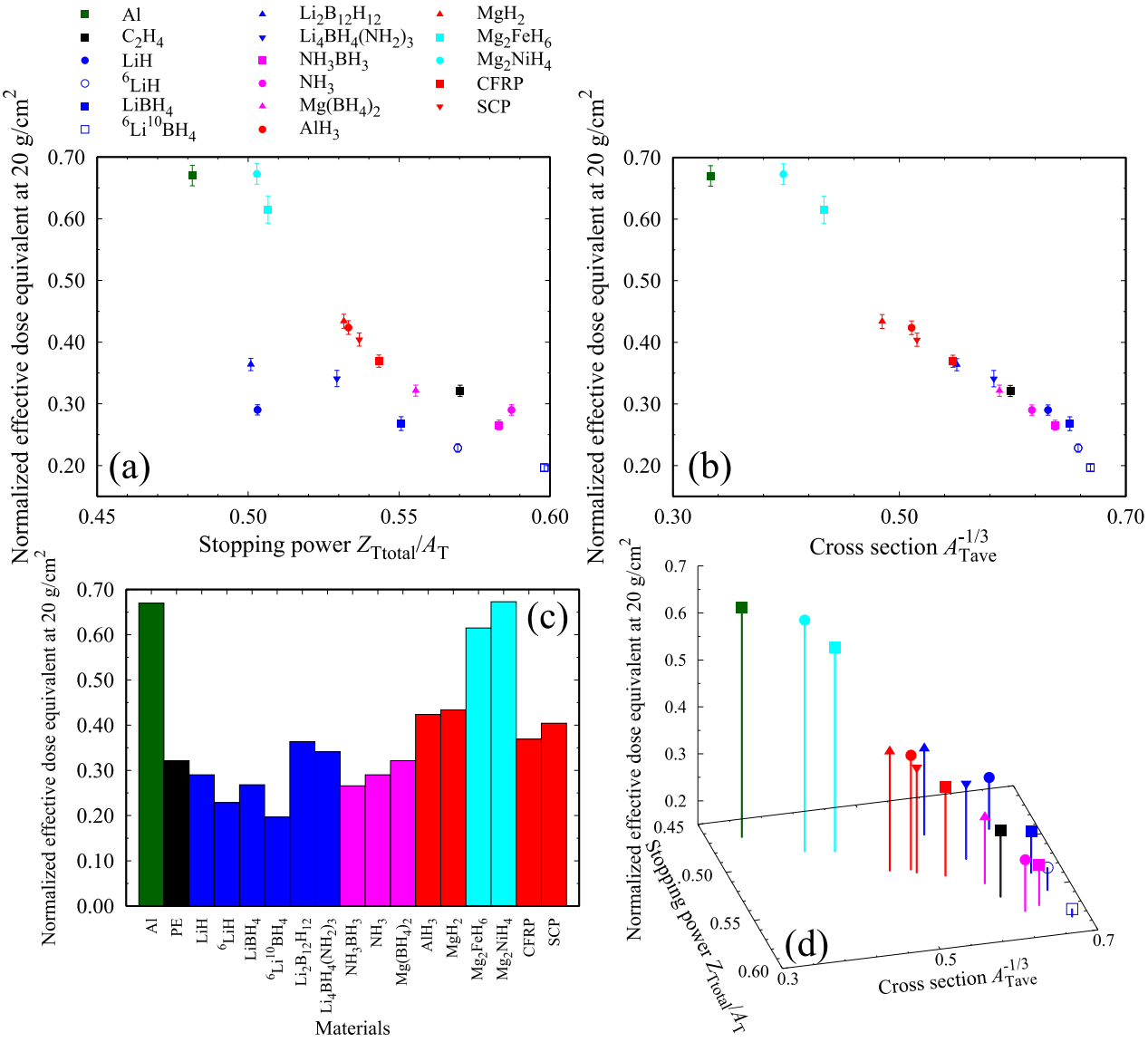

Figure 7. Scatter plots of (a) the stopping power parameter (Z_{Total}/A_T) and (b) fragmentation cross section parameter ($A_{Tave}^{-1/3}$) and the effective dose equivalent behind of the target materials of 20 g/cm^2 for 1 GeV/n Fe beam simulations. (c): Comparison of the normalized effective dose equivalent for each material. (d): Three dimensional view based on (a) and (b).

materials exhibited a high dose reduction rate of 73.4%. The dose reduction rates of composite materials, CFRP and SCP, in the group (iii) materials were 63.1% and 59.6%, respectively. These dose reduction rates were ~1.9 times better than conventional Al (33.0%). Composite materials have potential both for spacecraft construction as well as for effective shielding. The group (iv) materials, Mg_2FeH_6 and Mg_2NiH_4, did not provide significant dose reduction, being comparable to Al despite having higher shielding parameters. This is because the heavy nuclides (Fe and Ni) yield a lot of secondary particles via target fragmentation.

4. CONCLUSION

We have evaluated the effectiveness of several materials as shielding against space radiation as a function of two physical parameters, stopping power and nuclear fragmentation cross section using Geant4 Monte Carlo simulation. Fe ions are the heaviest particles in GCRs that contribute significantly to the effective dose equivalent in space. In the simulation, Fe ions at GCR-like energies were directed at shielding materials and the effective dose equivalent behind the materials was calculated Highly hydrogenous materials such as polyethylene and hydrides are compared to materials such as aluminum and complex hydrides including high Z metals with little or no hydrogen content. The dose due to secondary particles increases due to the fragmentation and then decreases due to loss of primary particles. $^6Li^{10}BH_4$ demonstrated the highest shielding efficiency, 1.2 times better than polyethylene. ^6LiH and NH_3BH_3 also were superior in shielding efficiency compared to polyethylene. Composite materials such as carbon fiber reinforced plastic and SiC composite plastic have shielding effectiveness of 1.9 times greater than aluminum; their mechanical strength makes them a good option for fabricating spacecraft structures. The stopping power and fragmentation cross section are useful parameters for investigating the properties of spacecraft shielding materials.

Declaration of Competing Interest

The authors declare that there are no potential conflicts of interest.

FUNDING

The work of authors at the National Institutes for Quantum and Radiological Science and Technology has been partially funded by Mitsubishi Heavy Industries, Ltd. Authors from Mitsubishi Heavy Industries, Ltd. own stock in the company.

References

Agostinelli, S., et al., 2003. Geant4—a Simulation Toolkit. Nucl. Instruments Methods A. 506 (3), 250–303. https://doi.org/10.1016/S0168-9002(03)01368-8.

Allison, J., et al., 2006. Geant4 Developments and Applications. IEEE Trans. Nucl. Sci. 53 (1), 270–278. https://doi.org/10.1109/TNS.2006.869826.

Allison, J., et al., 2016. Recent Developments in Geant4. Nucl. Instruments Methods A. 835, 186–225. https://doi.org/10.1016/j.nima.2016.06.125.

Ambrozova, I., et al., 2011. Monitoring on Board Spacecraft by Means of Passive Detectors. Radiat. Prot. Dosimetry 144 (1–4), 605–610. https://doi.org/10.1093/rpd/ncq305.

Andersson, B., et al., 1993. The FRITIOF Model for Very High Energy Hadronic Collisions. Zeitschrift Fur Phys. C Part. Fields 57 (3), 485–494. https://doi.org/10.1007/BF01474343.

Badhwar, G.D., et al., 1996. Intercomparison of Radiation Measurements on STS-63. Radiat. Meas. 26 (6), 901–916. https://doi.org/10.1016/S1350-4487(96)00082-0.

Ballarini, F., et al., 2006. GCR and SPE Organ Doses in Deep Space with Different Shielding: Monte Carlo Simulations Based on the FLUKA Code Coupled to Anthropomorphic Phantoms. Adv. Sp. Res. 37 (9), 1791–1797. https://doi.org/10.1016/j.asr.2006.03.007.

Beaujean, R., et al., 2002. Dosimetry inside MIR Station Using a Silicon Detector Telescope (DOSTEL). Radiat. Meas. 35 (5), 433–438. https://doi.org/10.1016/S1350-4487(02)00074-4.

Berger, T., et al., 2016. DOSIS & DOSIS 3D: Long-Term Dose Monitoring Onboard the Columbus Laboratory of the International Space Station (ISS). J. Sp. Weather Sp. Clim. 6, A39. https://doi.org/10.1051/swsc/2016034.

Bertini, H.W., 1969. Intranuclear-Cascade Calculation of the Secondary Nucleon Spectra from Nucleon-Nucleus Interactions in the Energy Range 340 to 2900 MeV and Comparisons with Experiment. Phys. Rev. 188 (4), 1711–1730. https://doi.org/10.1103/PhysRev.188.1711.

Brown, D.A., et al., 2018. ENDF/B-VIII.0: The 8 Th Major Release of the Nuclear Reaction Data Library with CIELO-Project Cross Sections, New Standards and Thermal Scattering Data. Nucl. Data Sheets 148, 1–142. https://doi.org/10.1016/j.nds.2018.02.001.

Chen, W.-C., 1997. Some Experimental Investigations in the Drilling of Carbon Fiber-Reinforced Plastic (CFRP) Composite Laminates. Int. J. Mach. Tools Manuf. 37 (8), 1097–1108. https://doi.org/10.1016/S0890-6955(96)00095-8.

Crusan, J.C., et al., 2018. Deep Space Gateway Concept: Extending Human Presence into Cislunar Space. 2018 IEEE Aerosp. Conf. 1–10. https://doi.org/10.1109/AERO.2018.8396541.

Cucinotta, F.A., 2014. Space Radiation Risks for Astronauts on Multiple International Space Station Missions. PLoS One 9 (4), e96099. https://doi.org/10.1371/journal.pone.0096099. edited by Paul Jaak Janssen.

Cucinotta, F.A., 2015. Review of NASA Approach to Space Radiation Risk Assessments for Mars Exploration. Health Phys 108 (2), 131–142. https://doi.org/10.1097/HP.0000000000000255.

DeWitt, J.M., et al., 2009. Assessment of Radiation Shielding Materials for Protection of Space Crews Using CR-39 Plastic Nuclear Track Detector. Radiat. Meas. 44 (9–10), 905–908. https://doi.org/10.1016/j.radmeas.2009.10.041.

Dobynde, M.I., Shprits, Y.Y., 2020. Radiation Environment Created with GCRs inside a Spacecraft. Life Sci. Sp. Res. 24, 116–121. https://doi.org/10.1016/j.lssr.2019.09.001.

Doke, T., et al., 2001. Measurements of LET-Distribution, Dose Equivalent and Quality Factor with the RRMD-III on the Space Shuttle Missions STS-84, -89 and -91. Radiat. Meas. 33 (3), 373–387. https://doi.org/10.1016/S1350-4487(00)00149-9.

Durante, M., 2014. Space Radiation Protection: Destination Mars. Life Sci. Sp. Res. 1, 2–9. https://doi.org/10.1016/j.lssr.2014.01.002.

English, R.A., et al., 1973. Apollo Experience Report- Protection Against Radiation. https://doi.org/10.1007/s13398-014-0173-7.2.

Giraudo, M., et al., 2018. Accelerator-Based Tests of Shielding Effectiveness of Different Materials and Multilayers Using High-Energy Light and Heavy Ions. Radiat. Res. 190 (5), 526. https://doi.org/10.1667/RR15111.1.

Guetersloh, S., et al., 2006. Polyethylene as a Radiation Shielding Standard in Simulated Cosmic-Ray Environments. Nucl. Instruments Methods B. 252 (2), 319–332. https://doi.org/10.1016/j.nimb.2006.08.019.

ICRP, 2013. Assessment of Radiation Exposure of Astronauts in Space. ICRP Publ. 123. Annu. ICRP 42 (4). https://doi.org/10.1016/j.icrp.2013.05.004.

Klerke, A., et al., 2008. Ammonia for Hydrogen Storage: Challenges and Opportunities. J. Mater. Chem. 18 (20), 2304. https://doi.org/10.1039/b720020j.

Kodaira, S., et al., 2013. Analysis of Radiation Dose Variations Measured by Passive Dosimeters Onboard the International Space Station during the Solar Quiet Period (2007–2008). Radiat. Meas. 49, 95–102. https://doi.org/10.1016/j.radmeas.2012.11.020.

Kodaira, S., et al., 2014. Verification of Shielding Effect by the Water-Filled Materials for Space Radiation in the International Space Station Using Passive Dosimeters. Adv. Sp. Res. 53 (1), 1–7. https://doi.org/10.1016/j.asr.2013.10.018.

Kodaira, S., et al., 2016. A Performance Test of a New High-Surface-Quality and High-Sensitivity CR-39 Plastic Nuclear Track Detector – TechnoTrak. Nucl. Instruments Methods B. 383, 129–135. https://doi.org/10.1016/j.nimb.2016.07.002.

Koi, T., 2010. New native QMD code in Geant4. In: Proc. MC2010 Monte Carlo Conf. Tokyo.

Matthiä, D., et al., 2013. A Ready-to-Use Galactic Cosmic Ray Model. Adv. Sp. Res. 51 (3), 329–338. https://doi.org/10.1016/j.asr.2012.09.022.

Miller, J., et al., 2003. Benchmark Studies of the Effectiveness of Structural and Internal Materials as Radiation Shielding for the International Space Station. Radiat. Res. 159, 381–390.

Orimo, S., et al., 2007. Complex Hydrides for Hydrogen Storage. Chem. Rev. 107 (10), 4111–4132. https://doi.org/10.1021/cr0501846.

Shavers, M.R., et al., 2004. Implementation of ALARA Radiation Protection on the ISS through Polyethylene Shielding Augmentation of the Service Module Crew Quarters. Adv. Sp. Res. 34 (6), 1333–1337. https://doi.org/10.1016/j.asr.2003.10.051.

La Tessa, C., et al., 2005. Fragmentation of 1GeV/Nucleon Iron Ions in Thick Targets Relevant for Space Exploration. Adv. Sp. Res. 35 (2), 223–229. https://doi.org/10.1016/j.asr.2005.02.007.

Wilson, J.W., et al., 1997. Shielding Strategies for Human Space Exploration. NASA Conf. Publicaition 3360.

Zeitlin, C, et al., 2005. Shielding and Fragmentation Studies. Radiat. Prot. Dosimetry 116 (1–4), 123–124. https://doi.org/10.1093/rpd/nci064.

Zeitlin, C., et al., 2006. Measurements of Materials Shielding Properties with 1GeV/Nuc 56Fe. Nucl. Instruments Methods B. 252 (2), 308–318. https://doi.org/10.1016/j.nimb.2006.08.011.

Zeitlin, C., et al., 2013. Measurements of Energetic Particle Radiation in Transit to Mars on the Mars Science Laboratory. Science (80-.) 340 (6136), 1080–1084. https://doi.org/10.1126/science.1235989.